HHS Public Access

Author manuscript

Nat Neurosci. Author manuscript; available in PMC 2014 December 01.

Published in final edited form as:

Nat Neurosci. 2014 June ; 17(6): 841–850. doi:10.1038/nn.3701.

Laminar-specific Scaling Down of Balanced Excitation and Inhibition in Auditory Cortex by Active Behavioral States

Mu Zhou[1,2,4,#], **Feixue Liang**[1,5,#], **Xiaorui R. Xiong**[1,4], **Lu Li**[5], **Haifu Li**[5], **Zhongju Xiao**[5,*], **Huizhong W. Tao**[1,3,*], and **Li I. Zhang**[1,2,*]

[1]Zilkha Neurogenetic Institute, University of Southern California, Los Angeles, CA 90089, USA

[2]Department of Physiology and Biophysics, University of Southern California, Los Angeles, CA 90089, USA

[3]Department of Cell and Neurobiology, University of Southern California, Los Angeles, CA 90089, USA

[4]Graduate Programs, Keck School of Medicine, University of Southern California, Los Angeles, CA 90089, USA

[5]Department of Physiology, School of Basic Medical Sciences, Southern Medical University, Guangzhou 510515, China

Abstract

Cortical sensory processing is modulated by behavioral and cognitive states. How the modulation is achieved through impacting synaptic circuits remains largely unknown. In awake mouse auditory cortex, we reported that sensory-evoked spike responses of layer 2/3 (L2/3) excitatory cells were scaled down with preserved sensory tuning when animals transitioned from quiescence to active behaviors, while L4 and thalamic responses were unchanged. Whole-cell voltage-clamp recordings further revealed that tone-evoked synaptic excitation and inhibition exhibited a robust functional balance. Changes of behavioral state caused scaling down of excitation and inhibition at an approximately equal level in L2/3 cells, but no synaptic changes in L4 cells. This laminar-specific gain control could be attributed to an enhancement of L1–mediated inhibitory tone, with L2/3 parvalbumin inhibitory neurons suppressed as well. Thus, L2/3 circuits can adjust the salience of output in accordance with momentary behavioral demands while maintaining the sensitivity and quality of sensory processing.

The processing of sensory information in cortical neurons is achieved through the spatiotemporal integration of converging synaptic inputs evoked by sensory inputs[1–3]. Such synaptic integration is largely determined by the structure of the underlying functional

*Correspondence should be addressed to: L.I.Zhang (liizhang@usc.edu), or Z.Xiao (xiaozj@fimmu.com), or H.W.Tao (htao@usc.edu).

#These authors contribute equally to this study.

Author Contributions

L.I.Z., Z.X. and H.W.T conceived and supervised the study. M.Z. and F.L performed all the experiments. L.L., H.L., and R.X. contributed to data collection. M.Z., F.L., H.W.T., and L.I.Z. performed data analysis. H.W.T. and L.I.Z. wrote the manuscript.

cortical synaptic circuits[2,4,5], but can also be influenced by behavioral and cognitive states of the animal[6–11] which modulate the internally generated brain activities[12–15]. In visual and somatosensory cortices, it has been shown that behaviorally active states, such as locomotion and whisking, result in a depolarization of the membrane potential and a more desynchronized state of cortical neurons[16–18], which alters the level or reliability of their spike responses to sensory stimulation[8,11,17–19]. Despite the observed changes in membrane potential dynamics, how behavioral states directly modulate cortical synaptic circuits, as reflected by potential changes of excitatory and inhibitory synaptic inputs to a cortical neuron, remains largely unknown.

In this study, by achieving high-quality *in vivo* whole-cell voltage-clamp recordings in awake head-fixed mice, we were able to reveal excitatory and inhibitory synaptic inputs to the same cortical neurons under different behavioral states of the animal. In middle layers of the primary auditory cortex (A1), our results revealed a robust functional balance between sound-evoked excitatory and inhibitory inputs to a cortical neuron under various behavioral states, which is a salient synaptic circuit property previously demonstrated in anesthetized animal models[2,20–23]. The balanced synaptic excitation and inhibition were found scaled down at a similar level during active states as compared to the quiet resting state in layer 2/3 but not layer 4 excitatory cells, resulting in well preserved sensory tuning of the former cells. We also provided evidence that layer 1 interneurons were activated in active states, which contributed to the reduced response gain of layer 2/3 excitatory cells. Together, our results suggest that balanced excitation and inhibition is a fundamental synaptic circuit basis for auditory cortical processing in the awake A1, and that behavioral state-dependent scaling of excitatory and inhibitory inputs may be a general strategy for cortical circuits to adjust the representation of sensory information according to momentary behavioral and task demands.

Results

Laminar-specific down-regulation of auditory responses

We first examined whether and how auditory cortical responses are modulated by changes of behavioral state in awake head-fixed mice habituated to rest or run on a flat rotatable plate (**Online Methods**). The behavior of the animal was monitored with a video camera, and the speed of the rotation of the plate was recorded in real time (Fig. 1a). The animal displayed three identifiable behavioral states (Fig. 1b): quiescence (“Q”, quiet resting), active without locomotion (“A – L”, whisking and/or facial/jaw/paw movements), and locomotion (“L”, running). During locomotion the mouse also whisked. These behavioral states correlated well with different speeds of plate rotation (Fig. 1b,c). “A – L” state caused small back and forth movements of the plate, the speed of which was clearly distinguished from that caused by locomotion (Fig. 1c). The power spectrum of the local field potential (LFP) recorded in the A1 (Fig. 1d) showed an increase in the power of high frequency oscillations (20–80 Hz) while a decrease in the power of low frequency oscillations (1–10 Hz) during both the “A – L” and “L” states as compared to the “Q” state (Fig. 1e,f, and Supplementary Fig. 1), consistent with previous reports that locomotion or whisking can result in a desynchronized brain state[11–13]. After determining the location of the primary auditory cortex (A1) with extracellular recordings, we performed *in vivo* cell-attached loose-

patch recordings from individual A1 neurons (**Online Methods**). Both the spontaneous and sound-evoked spikes of the cells were recorded. All the cells in this recorded population were presumed excitatory cells, since they all exhibited broad spike waveforms[24] (see insets in Fig. 1g,j for example spike waveforms). Compared to the "Q" state, "A – L" and "L" states similarly reduced the spontaneous firing rate in layer 2/3 (L2/3) neurons (Fig. 1g–i), but did not affect it in layer 4 (L4) neurons (Fig. 1j–l) (see Supplementary Fig. 2 for layer assignment). Such L2/3-specific decrease in spontaneous activity is reminiscent of a previous report in rat auditory cortex that spontaneous activity of superficial neurons is suppressed during cortical desynchronization[25]. Furthermore, "A – L" and "L" states similarly reduced the spiking response to the characteristic frequency (CF) tone in L2/3 neurons as compared to the "Q" state (Fig. 1m–o), whereas in L4 neurons the CF-tone evoked spiking activity was not affected by the changes of behavioral state (Fig. 1p–r). Thus, different from the observations in the visual cortex[11,18,19], where locomotion results in enhanced sensory-evoked activity in both layer 2/3 and layer 4, the auditory cortex exhibited a laminar-specific down-regulation of sensory-evoked responses. In addition, it is worth mentioning that both the spontaneous and evoked firing rates are higher in awake quiescence than urethane-anesthetized states (spontaneous: 2.29 ± 0.89 Hz for anesthesia, 4.06 ± 1.1 Hz for awake, $P < 0.05$, *t*-test; evoked: 50.2 ± 12.7 Hz for anesthesia, 60.2 ± 11.7 Hz for awake, $P < 0.05$, *t*-test, $n = 55$ and 32 respectively).

Behavioral state-dependent gain modulation

To determine the nature of the behavioral state-dependent modulation of auditory processing, we continuously mapped the frequency-intensity tonal receptive field (TRF) of spiking response in an individual cell by applying tone pips of different frequencies and intensities (Online **Methods**). Trials during active ("A") states were separated from those in quiescence. Since "A – L" state produced similar effects as locomotion (Fig. 1n,q), we did not further separate the trials in these two states. The spike TRF was reconstructed from at least ten complete sets of spike responses to 41 testing frequencies and 8 testing intensities. In the example L2/3 cell in Fig. 2a, "A" state apparently reduced the firing rates without affecting the overall shape of the spike TRF. Within the TRF, the average evoked spike number in an "A"-state trial strongly correlated with that in the corresponding "Q"-state trial (Pearson's correlation coefficient $r = 0.94$) (Fig. 2b), indicating that firing rates to different tone stimuli were reduced in proportion. In other words, firing rates were scaled down. The slope of the linear regression line (0.71) indicated an about 30% reduction in response gain (Fig. 2b). Concurrently, the onset of the evoked spike response was slightly delayed in "A" than "Q" state (Fig. 2c, arrows), together with a reduced level of spontaneous activity. In comparison, in the example L4 cell, "A" state did not apparently affect evoked or spontaneous firing rates or the shape of the TRF (Fig. 2d–f), with the slope of the linear regression line close to 1 (0.98, Fig. 2e). The onset delay of the evoked spike response was neither changed apparently (Fig. 2f).

In all the 17 recorded L2/3 excitatory cells, the evoked spike rate in "Q" state correlated well with that in "A" state (Fig. 2g). The slopes of the linear regression line for "A"-state versus "Q"-state responses were nearly all below 1, with a mean ± s.d. of 0.77 ± 0.14 (Fig. 2h). This indicates that the response gain of L2/3 excitatory cells was reduced in active states.

Most of these cells showed a 1–2 ms (1.5 ± 0.7 ms, mean ± s.d.) delay of spiking response onset in "A" state relative to "Q" state (Fig. 2i). In 10 of these cells, complete TRFs for both "A" and "Q" states were obtained. For these TRFs, no significant difference was observed for the characteristic frequency (Fig. 2j), the bandwidth at 20 dB above the intensity threshold (BW20, Fig. 2k), or the intensity threshold of TRF (Fig. 2l) between the two different states, indicating that the shape and sharpness of TRF remained the same despite the change in response gain. No correlation was found between the scaling factor and the cortical depth of recorded L2/3 cells (Supplementary Fig. 3). In comparison, in all the 15 recorded L4 cells, the slopes were close to 1 (1.02 ± 0.09, mean ± s.d.), indicating no change in response gain (Fig. 2m,n). The onset latency of evoked spiking response was overall unaffected by changes of behavioral state (Δlatency = 0.1 ± 0.8 ms, Fig. 2o), nor was the shape of spike TRF changed (Fig. 2p–r).

The absence of response changes in L4 suggests that activity of thalamic neurons may not change during active behaviors. To confirm this, we performed loose-patch recordings in the ventral part of the medial geniculate body (MGBv), the thalamic nucleus that provides direct feedforward input into the A1. Indeed, neither the spontaneous (Fig. 3a) nor the evoked spike responses of thalamic neurons (Fig. 3b) changed significantly from the "Q" to "A" state, indicating that auditory thalamic neurons were not directly affected by the behavioral changes.

Although the evoked firing rate of L2/3 cells was reduced in active states, their spontaneous activity was relatively more suppressed so that the signal-to-noise ratio (SNR), as defined by the ratio of evoked firing rate over spontaneous firing rate, was in fact increased (Fig. 3c). This increased SNR, together with the unchanged intensity threshold (Fig. 2l), indicates that the sensitivity of auditory processing was not reduced in active states despite the decreased response level.

Balanced excitation and inhibition in quiescent state

It remains unknown what are the properties of sound-driven synaptic excitation and inhibition to auditory cortical neurons in the awake brain, since previous studies have been mostly carried out in anesthetized preparations[2,20–23]. To understand the synaptic mechanisms underlying the observed behavioral state-dependent modulation of response gain, we performed whole-cell voltage-clamp recordings to reveal excitatory and inhibitory synaptic inputs to A1 neurons (Online **Methods**). We first examined properties of synaptic responses in quiescence. As shown by an example cell, a best-frequency (BF) tone elicited robust excitatory and inhibitory currents in the same cell (Fig. 4a). The major component of these currents could be best described as transient, as its temporal duration, as measured at the half-peak level (i.e. 50% duration), did not increase with increasing tone durations (Fig. 4b). In addition, the peak amplitude of synaptic currents did not increase either with increasing stimulus durations (Fig. 4c). The onset latency of inhibitory current was mostly delayed by 1–3 ms (1.95 ± 1.03 ms, mean ± s.d.) relative to that of the excitatory current evoked by the same stimulus (Fig. 4d), similar as what has been observed in anesthetized animals[20–23,26], and suggesting a fast feedforward nature of the inhibition[2,27]. The amplitude of inhibitory conductance was larger than that of the corresponding excitatory

conductance (Fig. 4e), with a mean E/I ratio of 0.42 ± 0.12 (Fig. 4f), which is in line with our previous studies in anesthetized animals[23,26,28,29]. We further compared the frequency tuning of excitation and inhibition at a moderate intensity level (40–50 dB sound pressure level, SPL). As shown by two example cells (Fig. 4g,h), the total frequency ranges for evoked excitatory and inhibitory currents were about the same, and the amplitude of excitatory current linearly correlated with that of the inhibitory current evoked by the same stimulus, resulting in very similar excitatory and inhibitory frequency tuning curves (Fig. 4g,h, inset). This finding suggests a functional balance of excitation and inhibition, i.e. the strength of inhibition co-varies with that of excitation. In a total of 15 recorded cells, we observed that the frequency range of excitation was not different from that of inhibition (Fig. 4i). The bandwidth of excitatory frequency tuning curve, as measured at the half-peak level (BW 50%), was not different from that of the inhibitory tuning curve of the same cell (Fig. 4j). Excitatory and inhibitory tuning curves also exhibited the same best frequency (Fig. 4k). Together, these results indicate that in awake A1 excitation and inhibition are balanced in the frequency domain, with inhibition temporally delayed briefly relative to excitation.

Scaling down of excitation and inhibition in active states

To examine how behavioral state regulates synaptic inputs, we applied best-frequency tones and varied their intensity in a random order. Responses were parsed into active state (including locomotion) and quiescence trials. As shown by an example L2/3 excitatory cell, the average excitatory current in response to BF tones increased in amplitude with increasing tone intensities (Fig. 5a). In the “A” state the excitatory currents to all tone intensities became smaller (Fig. 5a) in an approximately proportional manner (Fig. 5b, left and middle panel). The onset latencies of evoked excitatory currents were not changed significantly (Fig. 5b, right panel). The evoked inhibitory currents to different tone intensities were also reduced by a similar factor from the “Q” to “A” state, while the timing of inhibitory currents was not affected (Fig. 5c,d). In comparison, in a L4 excitatory cell, neither the excitatory nor inhibitory currents changed significantly in their amplitudes, nor were the onset latencies of these currents affected (Fig. 5e–h).

To examine state-dependent changes of synaptic responses in the frequency domain, we applied tone stimuli of different frequencies at a moderate intensity (40 or 50 dB SPL). As shown by an example L2/3 excitatory cell (Fig. 5i), tone-evoked excitatory and inhibitory currents were both reduced in amplitude from the “Q” to “A” state. The strong linear relationship between synaptic responses in the two states indicated a scaling of both excitatory and inhibitory inputs (Fig. 5j). Such coordinated modulation resulted in apparently unchanged frequency tuning of synaptic inputs, as demonstrated by the superimposed normalized synaptic tuning curves for “A” and “Q” states (Fig. 5i, inset). Consistent with the results of spiking response, in layer 4 we did not observe apparent effects of “A” state on the amplitude of either evoked excitatory or inhibitory synaptic responses (Fig. 5k,l). Together, the above results suggest that tone-evoked excitatory and inhibitory inputs to L2/3 cells were scaled down in behaviorally active states, thus preserving the functional balance between excitation and inhibition.

In all the 13 recorded L2/3 cells, we observed a strong linear correlation between evoked synaptic amplitudes in “A” and “Q” states for both excitation and inhibition (Fig. 5m), further demonstrating a scaling of excitatory and inhibitory responses by changes of behavior state. To determine the scaling factor, we calculated the ratio of peak response amplitude in “A” versus “Q” state for each tone-evoked response. As shown by the distribution of ratios for all the recorded neurons (Fig. 5n), in L2/3 the scaling factors were nearly all lower than 1 for both excitation and inhibition, with a mean ± s.d. of 0.64 ± 0.18 and 0.70 ± 0.18 respectively. In contrast, in L4 the scaling factors were 1.03 ± 0.11 and 1.01 ± 0.10 for excitation and inhibition respectively (Fig. 5n). We also quantified the scaling factor by the slope of the linear regression for peak response amplitudes in “A” versus “Q” state (Fig. 5o). The average slope was 0.65 ± 0.11 for excitation and 0.69 ± 0.13 for inhibition in L2/3 cells, while 1.02 ± 0.06 and 1.00 ± 0.02 respectively in L4 cells (Fig. 5o). Similar results were obtained when the charge transfer of synaptic currents was measured (Supplementary Fig. 4). When examined in the same cell, the slope for excitatory responses was similar as that for inhibitory responses (Fig. 5p). Therefore evoked excitation and inhibition in a L2/3 cell were reduced by a similar factor from the “Q” to “A” state, while excitation and inhibition in a L4 cell were not affected by changes of behavioral state (Fig. 5o). Finally, we argued that the reduction in recorded synaptic responses was not due to compromised recording quality during animal movements, as the linear current-voltage relationship of the cell remained as good in active states (Supplementary Fig. 5), and there was no obvious change in series resistance with animal movements (Supplementary Fig. 6). In addition, we found that the response amplitude to the same stimulus remained essentially unchanged before and after an epoch of animal movements and remained relatively stable from the start till the end of the recording sessions (Supplementary Fig. 7).

Change of membrane properties in active states

In visual cortex, locomotion is shown to cause a depolarization of neuronal membrane potential, which contributes to the increased visual responses[18,19]. Here, the reduced auditory responses suggested that the neuron’s membrane potential might be hyperpolarized instead. We thus recorded resting membrane potentials in current-clamp mode using a K^+-based internal solution (Online **Methods**) from L2/3 excitatory neurons. In the absence of sound stimulation, the membrane potential (V_m) fluctuated largely with occasional appearance of spontaneous spikes (Fig. 6a), but the distribution of potentials was statistically unimodal (Fig. 6b, $P > 0.05$, Hartigan’s dip test). In active states, the distribution shifted toward more hyperpolarized values (Fig. 6b), resulting in a more hyperpolarized mean V_m. In all similarly recorded cells ($N = 7$), the distribution of potentials was unimodal in both states, and the transition from the “Q” to “A” state resulted in a more hyperpolarized mean V_m (from −61.67 ± 1.83 mV to −64.75 ± 1.84 mV, Fig. 6c), as well as a reduction of V_m variability (Fig. 6d). In the meanwhile, the level of spike threshold remained constant (Fig. 6e). As a consequence, the probability of instantaneous V_m being within 10 mV of the spike threshold was reduced in “A” compared to “Q” state (Fig. 6f). This can contribute to the reduction of both spontaneous and evoked spiking activity of L2/3 neurons. Additionally, we found a reduction of baseline conductance from the “Q” to “A” state (Fig. 6g–i), which would result in an increase of input resistance of the cell. The decrease of baseline

conductance may be partly attributed to reduced spontaneous synaptic events as evidenced by the reduction of spontaneous spiking activity of L2/3 neurons (Fig. 1i).

Modulation of PV neuron activity

The reduced auditory evoked inhibition to L2/3 neurons in active states likely reflects reduced inhibitory neuron activity. It is known that the major source of inhibition to L2/3 excitatory cells is from the same layer[30]. Since parvalbumin (PV) expressing neurons most likely contribute to the feedforward inhibition in L2/3 excitatory cells[24] and play a major role in controlling the network gain because of their high firing rates and strong synaptic connections[24,31], we specifically examined PV neuron activity in different behavioral states. By injecting an AAV viral vector encoding Cre-dependent channelrhodopsin2 (ChR2) in PV-Cre mice (Fig. 7a and Online **Methods**), we were able to identify PV neurons with a previously described optogenetic method[32]. With loose-patch recordings, we actively searched for PV neurons, identification of which was based on their trains of spikes in response to a pulse of blue LED light applied to the A1 surface (Fig. 7b, left panel). These neurons responded robustly to tone stimuli (Fig. 7b, right panel). Consistent with previous reports with two-photon imaging guided loose-patch recordings[24,33], PV neurons exhibited shorter trough-to-peak intervals in their spike waveforms as compared to excitatory neurons (Fig. 7c,d). They also tended to have higher peak/trough amplitude ratios than excitatory cells (Fig. 7d). In L2/3, we found that both the spontaneous and evoked spiking activity of PV neurons was reduced from the “Q” to “A” state (Fig. 7e,f), whereas in L4 PV cell activity was not affected (Fig. 7g,h). These results suggest that the L2/3 networks comprising both excitatory and PV inhibitory neurons are generally suppressed by active behaviors.

Contribution of L1-mediated suppression

It has been shown previously that layer 1 plays a role in modulating activity in layer 2/3[Ref 17,34]. We then examined whether L1, which contains only inhibitory neurons[35,36], played a role in the behavioral state-dependent modulation of L2/3 activity. With loose-patch recordings, we found that L1 neurons were modulated by behavioral state differently from L2/3 and L4 cells: their spontaneous (Fig. 8a) as well as evoked (Fig. 8b) firing rates were both increased instead of decreased from the “Q” to “A” state. Since L1 neurons inhibit both excitatory and inhibitory cells in layer 2/3[Ref 34,37,38], the increased activity of L1 neurons may generally increase the inhibitory tone in the L2/3 network, leading to the reduced activity of L2/3 cells. To further confirm the involvement of L1, we silenced L1 spiking by applying 5 μM tetrodotoxin (TTX) to the A1 surface, following a previously published method[37]. We monitored auditory evoked multiunit spike responses in different layers before and after TTX application. As shown in Fig. 8c, within a limited time window (~ 150 s) after the topical application of TTX, the firing rate of L1 neurons gradually reduced to zero. Concurrently the evoked firing rate of L2/3 neurons increased to a stable level while that of L4 neurons remained unchanged. These results indicate that L1 spiking activity tonically suppressed L2/3 but not L4 neurons so that removing L1 inhibition increased firing rates of L2/3 cells. Beyond the time window, firing rates in L2/3 gradually reduced, indicating that L2/3 cells were also progressively affected by TTX. L4 neurons also progressively reduced their firing rates but with a delay. Therefore, the 150s window

provided a good opportunity to examine the effect of silencing L1 spikes, while leaving spikes in L2/3 and L4 unaffected by the drug. We next examined CF-tone evoked spikes in individual neurons with loose-patch recordings. Before TTX application, the L2/3 cells exhibited a normal reduction of response level from the "Q" to "A" state by 20.1 ± 6.9% (Fig. 8d,e). Within the 150 s window after the drug application, the response level in the "Q" state was increased by 19.2 ± 8.6% compared to that before the drug application (Fig. 8d). From the "Q" to "A" state, response level was reduced by only 4.1 ± 3.4%. Thus the behavioral state-dependent gain reduction was largely blocked when L1 spiking was silenced, supporting the notion that the increase of L1 firing rates in active states was responsible, at least partially, for the reduced response level in L2/3. As a control, the response level of L4 neurons was not affected by the drug application within the analysis time window, nor by the change of behavioral state (Fig. 8f), which is consistent with our earlier observations.

Discussion

How sensory processing in cerebral cortex is modulated by behavioral and cognitive states has been an important question for understanding the integrative function of the brain. To address this question, it is critical to examine how sensory-evoked responses in individual cortical neurons are modulated at cellular and synaptic levels. With the high-quality *in vivo* whole-cell voltage-clamp recordings, we were able to reveal the excitatory and inhibitory synaptic inputs to a cortical neuron under different behavioral states. Our results indicated a robust functional balance between synaptic excitation and inhibition in the awake A1, as manifested by the covariation of inhibitory and excitatory response amplitudes across different tone frequencies. Relative to quiescence, behaviorally active states scaled down excitatory and inhibitory inputs at a similar level in L2/3 but not L4 neurons, resulting in a proportional reduction of their spike responses to different tone stimuli. As a consequence, the sensory tuning of spike response as well as the functional balance between excitation and inhibition was preserved.

Behavioral state-dependent gain modulation

The observed suppression of auditory responses during active behaviors is reminiscent of a previous report that the animal's engagements in an auditory task result in reduced auditory cortical responses[10]. In the current study, the magnitude of the modulation is relatively small. The average effect on evoked spike responses is about 20% (Fig. 1o), while for some individual neurons it can be as high as 50%. Nevertheless, the moderate modulation effect may possibly change the information transfer in the A1 and consequently affect sound-dependent behaviors. This notion is supported by a study in the visual cortex showing that a moderate reduction in evoked firing rates caused by optogenetically activating PV inhibitory neurons can lead to a significant change in performance in visual detection tasks[39]. Our results contrast with observations in visual and somatosensory cortices that behaviorally active states depolarize the membrane potential of cortical neurons[16–19], and with the general thoughts that active states are characterized by an increase in excitatory and inhibitory conductances even in baseline conditions without sensory stimuli[40]. It is possible that the modulatory effect of behavioral state is specific to sensory modality. Or it may

depend on whether the specific sensory processing is engaged in the behavior that provides the modulation. Possibly during locomotion and whisking, the animal's exploration of the external environment depends more on visual and tactile than auditory perception. In accordance with this change in task demands, the relative salience of auditory information may be reduced.

Despite the reduction of response level, there is no change in the shape or size of TRFs of L2/3 neurons from quiescence to active states. And the intensity threshold and frequency tuning are well preserved. This is a result of gain modulation of spike responses, i.e. responses to different tone stimuli are scaled by a similar factor. Counterintuitively, the signal-to-noise ratio of auditory information in this output layer (L2/3) of A1 is in fact increased by about 35% in active states (Fig. 3c). The enhanced SNR is due to relatively more suppressed spontaneous activity than evoked activity, which is different from the observations in visual cortex that locomotion elevates SNR by enhancing sensory evoked responses[18,19], resulting in enhanced visual discrimination[19]. While the functional significance of this enhanced SNR in A1 remains to be examined with behavioral studies, our current results suggest that the sensitivity as well as the quality of auditory processing is at least maintained from quiescence to active states.

Balanced excitation and inhibition in awake cortex

Spectrotemporally balanced excitation and inhibition has been demonstrated previously in auditory cortical neurons of anesthetized animals, characterized by a similar frequency tuning of excitation and inhibition, a roughly constant ratio between excitatory and inhibitory response amplitudes across different stimuli, and a stereotypic temporal sequence of excitation briefly followed by inhibition[20–23]. The short interval (~ 2–3 ms) between the onsets of excitation and inhibition is consistent with a synaptic circuit dominant with feedforward inhibition[2,20,22]. Recently, an awake recording study in the visual cortex reports that while balanced excitation and inhibition is prevalent in the anesthetized cortex, in the awake cortex inhibition is much more broadly tuned than excitation in terms of spatial tuning[41]. Our current study in the auditory cortex however indicates that the functional balance between excitation and inhibition is ubiquitous across different brain states, and that this balance is actively preserved through a specific modulation of excitation and inhibition. The evoked synaptic excitation and inhibition are reduced by a similar factor from quiescence to active states. Such balanced scaling down of excitatory and inhibitory inputs would result in reduced output responses[42,43], as well as a longer integration time for spike generation[27] (see Fig. 2i). In addition, the scaled excitatory and inhibitory inputs suggest that the observed gain modulation of spike responses could be largely attributed to a network effect of suppression of L2/3 circuits, which results in a reduction of total evoked synaptic conductance. Together, our results strongly suggest that balanced excitation and inhibition is a fundamental synaptic circuit basis for auditory cortical processing in awake conditions.

L1 mediated suppression of L2/3 activity

Modulation of cortical activity may be achieved through bottom-up or top-down pathways[44]. Previously, it has been shown in mice that action potential firing in the

somatosensory thalamus increases during whisking, which drives the desynchronized state in the somatosensory cortex[45]. In this study, the absence of changes in spiking responses in L4 and MGBv neurons as well as in synaptic inputs to L4 cells argues that the behavioral state-dependent suppression of sensory responses in L2/3 of A1 is unlikely due to a modulation of neuronal activity in subcortical nuclei along the ascending auditory pathway. On the other hand, previous studies have suggested that behavior can affect network state through corticocortical inputs[17,46]. Corticocortical projections are known to ramify their axons in layer 1[Ref 47–50], which is in a good position to mediate state-dependent modulations of cortical activity in a top-down control. In this study, we found that L1 activity is increased from quiescence to active states. Since L1 activity can inhibit both excitatory and inhibitory cells in L2/3[Ref 34,37,38], the increased spiking of L1 neurons may generally enhance the inhibitory tone in the L2/3 network. This is evidenced by the increase of spike responses of L2/3 excitatory cells when spiking of L1 neurons is suppressed. Silencing of L1 spiking activity largely blocks the reduction of sensory evoked responses of L2/3 neurons when animals transition from quiescence to active states. This result indicates that the behavioral state-dependent gain modulation in the L2/3 network can be attributed, at least partially, to a direct regulation of L1-mediated inhibition.

Another possible way of modulating cortical activity is through neuromodulatory systems. In the mouse cortex, neuromodulatory projections such as cholinergic and noradrenergic fibers are distributed diffusely in all cortical layers without clear patterns (see the Allen Brain Atlas data portal at www.brain-map.org). In the visual cortex, the locomotion-induced depolarization of membrane potential and increase of firing rate is attributed to an effect of noradrenergic input, and is more or less uniform across L2/3 and L4[Ref 18], which is consistent with the diffuse pattern of noradrenergic fibers. In this study, the suppression of spontaneous and evoked responses induced by active behaviors is observed in L2/3 but not in L4. To our knowledge, there have not been reports about laminar-specific expression patterns of receptors for neuromodulators that are consistent with our current observations. Nevertheless our results do not exclude the possibility that the observed activity changes, including the enhancement of L1 activity, are mediated by effects of specific neuromodulators.

In summary, our study has demonstrated that a balanced scaling down of excitatory and inhibitory inputs underlies the suppressive gain modulation of sensory responses of L2/3 excitatory neurons induced by active behaviors. We postulate that scaling of synaptic inputs may be a simple strategy employed by brain circuits to maintain the quality of sensory processing while optimizing the level of salience of sensory information according to momentary behavioral demands.

Online Methods

Awake animal preparation

All experimental procedures used in this study were approved by the Animal Care and Use Committee at the University of Southern California. Female C57BL/6J mice aged 5–7 weeks were used in this study. Animals for awake recordings were prepared in a similar way as previously described[43,51]. Mice were housed with 12 hours light/dark cycle and with

flying saucer pet exercise wheels placed in their home cages. One week before the recording, the mouse was anesthetized with isoflurane (1.5%) and a screw for head fixation was mounted on top of the skull with dental cement. An adaptor for connecting to an enclosed sound delivery system was attached to the left ear. Afterward the mouse was injected subcutaneously with 0.1mg/kg buprenorphine and returned to its home cage. During the recovery period, the mouse was trained to get accustomed to the head fixation on the recording setup. To fix the head, the screw was tightly fit into a metal post. The animal was allowed to run freely on a flat plate rotating smoothly around its center. On the day of recording, the mouse was anesthetized with isoflurane. Surgery was performed in a sound-attenuation booth (Acoustic Systems). Craniotomy over the A1 region was performed and the dura was removed. The animal was positioned with the left ear connected to a calibrated closed acoustic delivery system using a TDT EC1 speaker. The right ear was plugged. Multi-unit recordings were made with a tungsten electrode (2 MΩ, FHC) to identify the A1 based on response properties and the tonotopic gradient, as described in previous studies[52]. The animal head was tilted so that the electrode could penetrate the A1 surface at an angle of 80°. The animal was allowed to recover from isoflurane for at least 1 hour. Recording was started after the animal exhibited normal running. The recording session lasted for about 4 hours. The animal was given drops of 5% sucrose through a pipette every hour.

In vivo whole-cell and loose-patch recordings in awake animals

Whole-cell recordings were made with an Axopatch 200B amplifier (Molecular Devices). Patch pipettes (impedance of 4–5 MΩ) contained a cesium-based solution (in mM): 125 Cs-gluconate, 5 TEA-Cl, 4 MgATP, 0.3 GTP, 10 phosphocreatine, 10 HEPES, 10 EGTA, 2 CsCl, 1.5 QX-314, 1% biocytin or 0.25 fluorescent dextrans, pH 7.3. The patch pipette, controlled by a micromanipulator (Siskiyou), was lowered into the A1 at the same angle as in multi-units recordings. The cortical surface was covered with 3.5% agar prepared in a warm artificial cerebrospinal fluid (ACSF; containing in mM: NaCl 124, NaH_2PO4 1.2, KCl 2.5, $NaHCO_3$ 25, Glucose 20, $CaCl_2$ 2, $MgCl_2$ 1). Whole cell capacitance was fully compensated and the initial series resistance (R_s; 15–50 MΩ) was compensated for 40–60% to achieve an effective R_s of 10–30 MΩ;. For some recordings, we regularly monitored R_s before, during and after epochs of animal movements. The running epochs were relatively evenly spaced during each of recording sessions, which usually last for less than 10 minutes, enough for us to collect data for different states. There was no significant change (< 10%) of R_s during our effective recording sessions (see Supplementary Fig. 6 & 7). Signals were low pass filtered at 2 kHz and sampled at 10 kHz. Only cells with resting membrane potential lower than −50 mV were studied. A −10 mV junction potential was corrected. Excitatory and inhibitory synaptic currents were recorded under the voltage-clamp mode with the cell clamped at −70 mV and 0 mV respectively. Membrane potentials were recorded under the current-clamp mode with pipettes containing a potassium-based solution (in mM): 130 K-gluconate, 4 MgATP, 0.3 GTP, 8 phosphocreatine, 10 HEPES, 10 EGTA, 5 KCl, 1 $CaCl_2$, 0.25 fluorescein dextran, pH 7.3. Signals were low pass filtered at 5 kHz and sampled at 10 kHz. As demonstrated before[23,26,53], the blind whole-cell recording method with relatively large pipette openings resulted in almost exclusive sampling from excitatory cortical neurons. Loose-patch recordings were performed as previously described[54], with a pipette filled with ACSF. Signals were recorded in voltage-clamp, with a command voltage applied

to adjust the baseline current to be zero. Loose-patch recordings from MGBv neurons were made by vertically penetrating the brain (2.8 ~ 3.6 mm from Bregma, 1.7 ~ 2.2 mm from midline, 2.8 ~ 3.2 mm below the pia surface). MGBv was discriminated from other auditory thalamic regions as previously described[54]. LFP recordings were made with the same recording pipette as in loose-patch recordings. During recordings, behaviors of the animal were recorded with a video camera. The rotating speed (without distinguishing the rotation direction) of the plate was detected with an optical sensor and recorded simultaneously. The behavioral and rotating speed recordings were precisely timed with the electrophysiological recording. The behavioral state of the animal was analyzed both online and offline.

On average, one good whole-cell recording (maintained for 20–40 minutes) or two loose-patch recordings (maintained for more than 1 hour) was obtained in each well-trained animal. The recording sites were marked. The laminar locations of the recorded neurons were determined based on the micromanipulator reading, and in some cases confirmed by histology of the track of pipette penetration and/or fluorescence or biocytin labeled cell bodies. We found a relatively good correspondence between the traveling depth of the recording pipette from the pia and the reconstructed laminar location of the recorded neuron (see Supplementary Fig. 1). The depth range of different layers in mouse A1 was determined based on the results from Nissl staining and fluorescence expression pattern in a L4-specific Cre line (Scnn1a-Tg3-cre, Jackson Laboratory) crossed with the Ai14 reporter mouse (see Supplementary Fig. 1a). The L2/3 neurons were sampled at a cortical depth of 250–350 μm from the pial surface, L4 neurons at a depth of 375–500 μm[54], and L1 neurons were within 100 μm from the pia.

Optogenetically guided loose-patch recordings from PV neurons

Adult PV-Cre (Jackson Laboratory) female mice were anesthetized with 1.5% isoflurane. A small cut was made on the skin covering the right A1 and the muscles were removed. Two ~0.2 mm craniotomies were made in the A1 region (temporal lobe, 2.7 and 3.2 mm caudal to Bregma). Adeno-associated viruses (AAVs) encoding ChR2 were purchased from the University of Pennsylvania Viral Vector Core: AAV2/9.EF1α.DIO.hChR2(H134R)-EYFP.WPRE.hGH (Addgene 20298). The virus was delivered using a beveled glass micropipette (tip diameter: ~40 μm) attached to a microsyringe pump (World Precision Instruments). Injections were performed at two locations and two depths (300 and 600 μm), at a volume of 100 nl per injection and at a rate of 20 nl min^{-1}. Right after each injection, the pipette was allowed to rest for 4 minutes before withdrawal. We then sutured the scalp, injected 0.1 mg kg^{-1} buprenorphine and returned the mouse to its home cage. Mice were allowed to recover for 3–4 weeks. On the day of recording, loose-patch recordings using pipettes of smaller tip openings (pipette impedance ~10 MΩ) were performed. An optic fiber connecting to a blue LED source (470 nm, Thorlabs) was positioned close to the cortical surface of the recording site. We actively searched for neurons exhibiting LED evoked spikes, which were identified as PV neurons. After each experiment that brain was sectioned and imaged to confirm the expression of ChR2-EYFP.

Silencing L1 with TTX

This method was adapted from a previous study[37]. Firstly we examined the time course of TTX effects in each layer. A glass pipette containing 1 M NaCl was used for recording multi-unit spikes. Multi-unit recording was made at 70 μm (L1), 250 μm (L2/3) or 425 μm (L4) below the pia surface of the A1. Responses to repetitive 50 dB CF tones (ISI = 4 s) were measured before and after TTX application. TTX solution (5 μM) was applied through a glass micropipette (~100 μm opening) attached via polyethylene tubing to a syringe. Each time we loaded ~ 2 μl TTX in the pipette and applied a very small pressure so that the TTX solution could be gently applied onto the A1 surface. To determine the contribution of L1 activity to gain changes in L2/3, loose-patch recordings were performed in L2/3 or L4, while the behavior and running speed of the animal were simultaneously recorded. Responses to repetitive 50 dB CF tones (ISI = 2 s) were measured before and after TTX application. Spike responses during a ~ 150 seconds window after TTX application when L2/3 firing rates became stable were analyzed and compared to responses before TTX application.

Sound stimulation

Software for sound stimulation and data acquisition was custom-developed in LabVIEW (National Instruments). For loose-patch recordings, pure tones (2–32 kHz spaced at 0.1 octave, 50-ms duration, 3-ms ramp) at eight intensities (0–70 dB SPL spaced at 10 dB) were delivered pseudo-randomly. Inter-stimulus interval (ISI) was 0.5 s. Spike TRFs were continuously mapped to obtain TRFs in different states. It took ~2.5 hours to map TRFs for more than 50 repetitions, from which we were able to reconstruct TRFs of about 10 repetitions for active states. For whole-cell recordings, either best frequency tones at seven sound intensities (10–70 dB SPL spaced at 10 dB) were delivered randomly with ISI = 2 s, or 40-dB tones at twenty-one frequencies (2–32 kHz, spaced at 0.2 octave) were delivered pseudo-randomly with ISI = 1 s. Thus, data collection was randomized.

Data analysis

We performed data analysis with custom-developed software (MATLAB, MathWorks). Analysis performers were partially blind to the conditions of the experiments, since the data from all the recorded neurons were first pooled together for a randomized batch processing without categorizing the neurons according to their laminar locations.

Behavioral state

The three behavioral states (Fig. 1b), quiescence (“Q”), active without locomotion (“A – L”), and locomotion (“L”), were identified based on the body movement and the rotation speed of the plate. In “Q” state, there was no obvious body movement and the average rotation speed (in each 1-s epoch) was lower than 0.5 cm s^{-1}. Animal normally stayed in “Q” state for more than 70% of the recording time. In “A – L” state, the animal showed whisking and/or facial/jaw/paw movements, which caused small back and forth movements of the plate with an average speed below 2 cm s^{-1}. In “L” state, the animal was running forward, with the rotating speed consistently above 2 cm s^{-1}. During locomotion the mouse also whisked. The two active states each will take about 10% of the recording time. Well

trained animals to spend relatively more time on running. In a typical experiment, quiescence and active states of the animal were intermingled (see Supplementary Fig. 7a).

Extracellular signals

LFP signals were low-pass filtered at 300 Hz. After fast Fourier transformation of the signal, normalized power spectrum was obtained and power ratio was calculated as the ratio of the area under 1~10 Hz band over that under 20~80 Hz band. Loose-patch recording signals were filtered with a 100–5000 Hz band-pass filter. Spontaneous firing rates were calculated from spikes within a 200 ms window before tone onsets, or within 6-s segments of records during which only spontaneous spikes were recorded. Spike TRF was determined as the frequency-intensity space where firing rates exceeded the average spontaneous level by 2 s.d. of baseline fluctuations. Evoked firing rates were calculated by subtracting the average spontaneous firing rate. CF was defined as the frequency at which tones evoked a significant spike response with minimum intensity. This minimum intensity was the intensity threshold of TRF. PSTHs were derived from CF-tone evoked responses. Spike response latency was defined as the lag between the stimulus onset and the time point in the PSTH where evoked firing rate exceeded the average spontaneous firing rate by 2 s.d. of baseline activity. Signal-to-noise ratio (SNR) was calculated for CF-tone evoked responses as the evoked firing rate within a 50 ms time window following the tone onset divided by the average spontaneous firing rate.

Synaptic responses

Synaptic response traces evoked by the same test stimuli were averaged separately for each behavior state. Synaptic onset latency was determined at the time point where the evoked current exceeded the average baseline by 2 s.d.. Peak amplitude was determined by averaging within a 5 ms window centered at the response peak after subtracting baseline current. Charge transfer was calculated by summing up the current values within the evoked response time window after subtracting baseline current. Excitatory and inhibitory synaptic conductances were derived according to $\Delta I = G_e * (V - E_e) + G_i * (V - E_i)$. ΔI is the amplitude of the synaptic current at any time point after subtracting the average baseline current specific to each behavior state; G_e and G_i are the excitatory and inhibitory synaptic conductance; V is the holding voltage, and E_e (0 mV) and E_i (−70 mV) are the reversal potentials. The clamping voltage V was corrected from the applied holding voltage (V_h): $V = V_h - R_s * I$, where R_s is the effective series resistance. By holding the recorded cell at two different voltages (the reversal potentials for excitatory and inhibitory current respectively), G_e and G_i could be resolved from the equation[23,26,29,55,56]. Resting conductance was calculated based on the average baseline currents within a 50 ms window before the onset of evoked currents recorded under two different voltages (−70 mV and 0 mV).

To determine frequency tuning, peak amplitudes of synaptic inputs at different frequencies were fit with an envelope curve using a MATLAB software Envelope 1.1 (developed by Lei Wang, MathWorks), as previously described[29]. Total frequency range and BW50% were defined as the bandwidths of the fitted envelope curve at 10% and 50% of maximum level respectively. BF was defined as the frequency corresponding to the maximum of the fitted envelope curve.

Statistics

Shapiro-Wilk test were first applied to exam whether samples had a normal distribution. In the case of a normal distribution, *t*-test or ANOVA test was applied. Otherwise, a non-parametric test (Wilcoxon signed-rank test in this study) was applied. Data were presented as mean ± s.d. if not otherwise specified. In this study, all the representative cases are followed by a population summary to demonstrate the repeatability. No statistical test was run to determine sample size a priori. The sample sizes we chose are similar to those used in previous publications. Since for many cells, responses of the same recorded neuron in different states were tested for multiple (>10) times, paired *t*-test or Wilcoxon signed-rank test was also performed on an individual-cell basis. The results were generally consistent with the group comparison. For the linear regression, both the correlation coefficient ("*r*") and *P* value were calculated to evaluate the strength and significance of the linear correlation. "*r*" values were indicated for individual linear regressions and summarized in Fig. 2g and Fig. 5m. For all the L2/3 neurons in Fig. 2, *P* values for the correlation between responses in two states (similar as in Fig. 2b) were all lower than 1×10^{-9}. *P* values for the correlation between excitatory and inhibitory responses of the neurons in Fig. 4 (similar as in Fig. 4g) were all lower than 1×10^{-8}. *P* values for the correlation between synaptic responses in two different states in Fig. 5 were all lower than 1×10^{-5}.

A supplementary methods checklist is available.

Supplementary Material

Refer to Web version on PubMed Central for supplementary material.

Acknowledgement

This work was supported by grants to L.I.Z. from the US National Institutes of Health (NIH; R01DC008983) and the David and Lucile Packard Foundation (Packard Fellowships for Science and Engineering). H.W.T. was supported by an NIH grant R01EY019049. Z.X., L.I.Z., and F.L. were supported by China NSF grants (U1301225, 31228013, 31200831). We thank Brian Zingg and Ling-yun Li for the help on viral injection and Nissl-staining.

References

1. Oswald AM, Schiff ML, Reyes AD. Synaptic mechanisms underlying auditory processing. Current opinion in neurobiology. 2006; 16:371–376. [PubMed: 16842988]
2. Wu GK, Tao HW, Zhang LI. From elementary synaptic circuits to information processing in primary auditory cortex. Neuroscience and biobehavioral reviews. 2011; 35:2094–2104. [PubMed: 21609731]
3. Petersen CC, Crochet S. Synaptic computation and sensory processing in neocortical layer 2/3. Neuron. 2013; 78:28–48. [PubMed: 23583106]
4. Callaway EM. Local circuits in primary visual cortex of the macaque monkey. Annual review of neuroscience. 1998; 21:47–74.
5. Douglas RJ, Martin KA. Neuronal circuits of the neocortex. Annual review of neuroscience. 2004; 27:419–451.
6. Fanselow EE, Nicolelis MA. Behavioral modulation of tactile responses in the rat somatosensory system. J Neurosci. 1999; 19:7603–7616. [PubMed: 10460266]
7. Reynolds JH, Chelazzi L. Attentional modulation of visual processing. Annual review of neuroscience. 2004; 27:611–647.

8. Ferezou I, et al. Spatiotemporal dynamics of cortical sensorimotor integration in behaving mice. Neuron. 2007; 56:907–923. [PubMed: 18054865]
9. Lee S, Carvell GE, Simons DJ. Motor modulation of afferent somatosensory circuits. Nature neuroscience. 2008; 11:1430–1438. [PubMed: 19011625]
10. Otazu GH, Tai LH, Yang Y, Zador AM. Engaging in an auditory task suppresses responses in auditory cortex. Nature neuroscience. 2009; 12:646–654. [PubMed: 19363491]
11. Niell CM, Stryker MP. Modulation of visual responses by behavioral state in mouse visual cortex. Neuron. 2010; 65:472–479. [PubMed: 20188652]
12. Crochet S, Petersen CC. Correlating whisker behavior with membrane potential in barrel cortex of awake mice. Nature neuroscience. 2006; 9:608–610. [PubMed: 16617340]
13. Poulet JF, Petersen CC. Internal brain state regulates membrane potential synchrony in barrel cortex of behaving mice. Nature. 2008; 454:881–885. [PubMed: 18633351]
14. Goard M, Dan Y. Basal forebrain activation enhances cortical coding of natural scenes. Nature neuroscience. 2009; 12:1444–1449. [PubMed: 19801988]
15. Constantinople CM, Bruno RM. Effects and mechanisms of wakefulness on local cortical networks. Neuron. 2011; 69:1061–1068. [PubMed: 21435553]
16. Gentet LJ, Avermann M, Matyas F, Staiger JF, Petersen CC. Membrane potential dynamics of GABAergic neurons in the barrel cortex of behaving mice. Neuron. 2010; 65:422–435. [PubMed: 20159454]
17. Zagha E, Casale AE, Sachdev RN, McGinley MJ, McCormick DA. Motor cortex feedback influences sensory processing by modulating network state. Neuron. 2013; 79:567–578. [PubMed: 23850595]
18. Polack PO, Friedman J, Golshani P. Cellular mechanisms of brain state-dependent gain modulation in visual cortex. Nature neuroscience. 2013; 16:1331–1339. [PubMed: 23872595]
19. Bennett C, Arroyo S, Hestrin S. Subthreshold mechanisms underlying state-dependent modulation of visual responses. Neuron. 2013; 80:350–357. [PubMed: 24139040]
20. Wehr M, Zador AM. Balanced inhibition underlies tuning and sharpens spike timing in auditory cortex. Nature. 2003; 426:442–446. [PubMed: 14647382]
21. Zhang LI, Tan AYY, Schreiner CE, Merzenich MM. Topography and synaptic shaping of direction selectivity in primary auditory cortex. Nature. 2003; 424:201–205. [PubMed: 12853959]
22. Tan AY, Zhang LI, Merzenich MM, Schreiner CE. Tone-evoked excitatory and inhibitory synaptic conductances of primary auditory cortex neurons. J Neurophysiol. 2004; 92:630–643. [PubMed: 14999047]
23. Wu GK, Arbuckle R, Liu BH, Tao HW, Zhang LI. Lateral sharpening of cortical frequency tuning by approximately balanced inhibition. Neuron. 2008; 58:132–143. [PubMed: 18400169]
24. Li LY, et al. Differential Receptive Field Properties of Parvalbumin and Somatostatin Inhibitory Neurons in Mouse Auditory Cortex. Cereb Cortex. 2014
25. Sakata S, Harris KD. Laminar-dependent effects of cortical state on auditory cortical spontaneous activity. Frontiers in neural circuits. 2012; 6:109. [PubMed: 23267317]
26. Zhou Y, et al. Preceding Inhibition Silences Layer 6 Neurons in Auditory Cortex. Neuron. 2010; 65:706–717. [PubMed: 20223205]
27. Zhou Y, et al. Generation of spike latency tuning by thalamocortical circuits in auditory cortex. J Neurosci. 2012; 32:9969–9980. [PubMed: 22815511]
28. Wu GK, Li P, Tao HW, Zhang LI. Nonmonotonic synaptic excitation and imbalanced inhibition underlying cortical intensity tuning. Neuron. 2006; 52:705–715. [PubMed: 17114053]
29. Sun YJ, et al. Fine-tuning of pre-balanced excitation and inhibition during auditory cortical development. Nature. 2010; 465:927–U928. [PubMed: 20559386]
30. Dantzker JL, Callaway EM. Laminar sources of synaptic input to cortical inhibitory interneurons and pyramidal neurons. Nature neuroscience. 2000; 3:701–707. [PubMed: 10862703]
31. Pfeffer CK, Xue M, He M, Huang ZJ, Scanziani M. Inhibition of inhibition in visual cortex: the logic of connections between molecularly distinct interneurons. Nature neuroscience. 2013; 16:1068–1076. [PubMed: 23817549]

32. Lima SQ, Hromadka T, Znamenskiy P, Zador AM. PINP: a new method of tagging neuronal populations for identification during in vivo electrophysiological recording. PloS one. 2009; 4:e6099. [PubMed: 19584920]
33. Ma WP, et al. Visual representations by cortical somatostatin inhibitory neurons--selective but with weak and delayed responses. J Neurosci. 2010; 30:14371–14379. [PubMed: 20980594]
34. Jiang X, Wang G, Lee AJ, Stornetta RL, Zhu JJ. The organization of two new cortical interneuronal circuits. Nature neuroscience. 2013; 16:210–218. [PubMed: 23313910]
35. Winer JA, Larue DT. Populations of GABAergic neurons and axons in layer I of rat auditory cortex. Neuroscience. 1989; 33:499–515. [PubMed: 2636704]
36. Hestrin S, Armstrong WE. Morphology and physiology of cortical neurons in layer I. J Neurosci. 1996; 16:5290–5300. [PubMed: 8757242]
37. Shlosberg D, Amitai Y, Azouz R. Time-dependent, layer-specific modulation of sensory responses mediated by neocortical layer 1. J Neurophysiol. 2006; 96:3170–3182. [PubMed: 17110738]
38. Wozny C, Williams SR. Specificity of synaptic connectivity between layer 1 inhibitory interneurons and layer 2/3 pyramidal neurons in the rat neocortex. Cereb Cortex. 2011; 21:1818–1826. [PubMed: 21220765]
39. Glickfeld LL, Histed MH, Maunsell JH. Mouse primary visual cortex is used to detect both orientation and contrast changes. J Neurosci. 2013; 33:19416–19422. [PubMed: 24336708]
40. Destexhe A, Rudolph M, Pare D. The high-conductance state of neocortical neurons in vivo. Nature reviews. Neuroscience. 2003; 4:739–751. [PubMed: 12951566]
41. Haider B, Hausser M, Carandini M. Inhibition dominates sensory responses in the awake cortex. Nature. 2013; 493:97–100. [PubMed: 23172139]
42. Liu BH, et al. Broad inhibition sharpens orientation selectivity by expanding input dynamic range in mouse simple cells. Neuron. 2011; 71:542–554. [PubMed: 21835349]
43. Xiong XR, et al. Interaural level difference-dependent gain control and synaptic scaling underlying binaural computation. Neuron. 2013; 79:738–753. [PubMed: 23972599]
44. Harris KD. Top-down control of cortical state. Neuron. 2013; 79:408–410. [PubMed: 23931991]
45. Poulet JF, Fernandez LM, Crochet S, Petersen CC. Thalamic control of cortical states. Nature neuroscience. 2012; 15:370–372. [PubMed: 22267163]
46. Nelson A, et al. A circuit for motor cortical modulation of auditory cortical activity. J Neurosci. 2013; 33:14342–14353. [PubMed: 24005287]
47. Felleman DJ, Van Essen DC. Distributed hierarchical processing in the primate cerebral cortex. Cereb Cortex. 1991; 1:1–47. [PubMed: 1822724]
48. Cauller LJ, Clancy B, Connors BW. Backward cortical projections to primary somatosensory cortex in rats extend long horizontal axons in layer I. J Comp Neurol. 1998; 390:297–310. [PubMed: 9453672]
49. Gonchar Y, Burkhalter A. Distinct GABAergic targets of feedforward and feedback connections between lower and higher areas of rat visual cortex. J Neurosci. 2003; 23:10904–10912. [PubMed: 14645486]
50. Petreanu L, Mao T, Sternson SM, Svoboda K. The subcellular organization of neocortical excitatory connections. Nature. 2009; 457:1142–1145. [PubMed: 19151697]
51. Olsen SR, Bortone DS, Adesnik H, Scanziani M. Gain control by layer six in cortical circuits of vision. Nature. 2012; 483:47–52. [PubMed: 22367547]
52. Guo W, et al. Robustness of cortical topography across fields, laminae, anesthetic states, and neurophysiological signal types. J Neurosci. 2012; 32:9159–9172. [PubMed: 22764225]
53. Li YT, Ibrahim LA, Liu BH, Zhang LI, Tao HW. Linear transformation of thalamocortical input by intracortical excitation. Nature neuroscience. 2013; 16:1324–1330. [PubMed: 23933750]
54. Li LY, Li YT, Zhou M, Tao HW, Zhang LI. Intracortical multiplication of thalamocortical signals in mouse auditory cortex. Nature neuroscience. 2013; 16:1179–1181. [PubMed: 23933752]
55. Borg-Graham LJ, Monier C, Fregnac Y. Visual input evokes transient and strong shunting inhibition in visual cortical neurons. Nature. 1998; 393:369–373. [PubMed: 9620800]
56. Anderson JS, Carandini M, Ferster D. Orientation tuning of input conductance, excitation, and inhibition in cat primary visual cortex. J Neurophysiol. 2000; 84:909–926. [PubMed: 10938316]

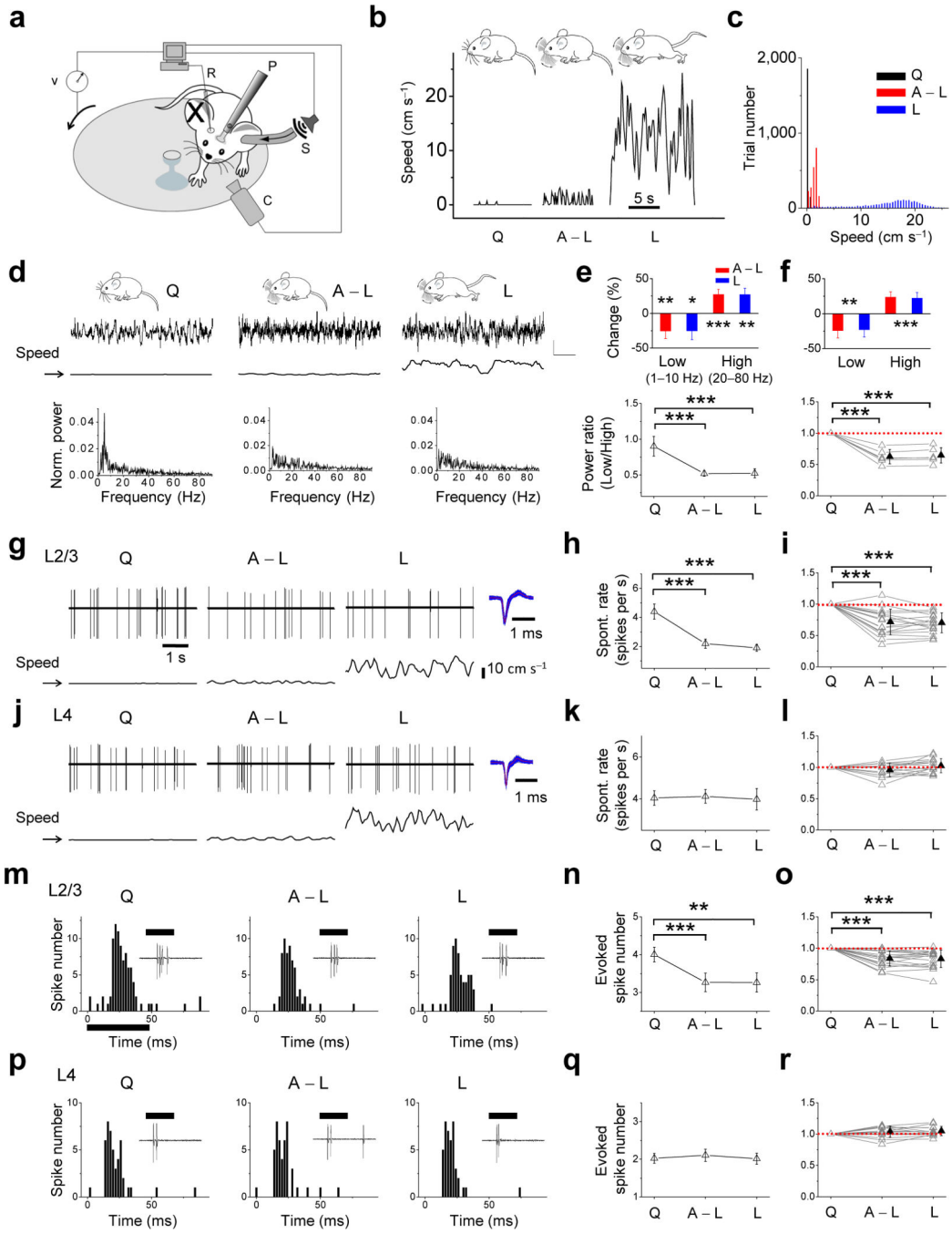

Figure 1.

Behavioral state-dependent modulation of spike responses in the mouse A1. (**a**) Experimental setup. R, recording electrode; P, head-fixation post; S, sound stimulation; C, camera; v, velocity meter. (**b**) Sample records of plate rotation speed in different behavioral states. “Q”, quiescence; “A – L”, active without locomotion; “L”, locomotion. (**c**) Distribution of average speeds (within a 1 sec epoch) in randomly sampled 2000 epochs (*n* = 3 animals). (**d**) Top, sample records of LFP in the A1. Scale: 250 μV and 0.5 s. Middle, simultaneously recorded plate rotating speed. Arrow indicates speed at 0. Scale: 20 cm s^{-1}

and 0.5 s. Bottom, power spectrum of LFP. (**e**) Top, percentage change in power of low-frequency (1–10 Hz) and high-frequency (20–80 Hz) components of LFP relative to quiescence, for the recording in (**d**). Power spectrums were generated for each 3.3 sec segment of LFP records. Bar = s.d. $N = 5$ segments. From left to right, *t*-test (**$P = 0.0035$, $t = -5.118$), Wilcoxon signed rank test (*$P = 0.0313$, $Z = -1.888$), *t*-test (***$P = 0.0006$, $t = 8.268$), *t*-test (**$P = 0.0012$, $t = 6.865$). Bottom, the ratio of power of the low versus high-frequency component. One-way ANOVA ($P = 6.68\times10^{-6}$, $F = 37.73$) and post hoc test (**$P < 0.01$, ***$P < 0.001$, same for the below). (**f**) Summary of recordings in 6 animals. Power ratio was normalized by the average value in the "Q" state. Top, *t*-test (**$P = 0.0011$, 0.0016, ***$P = 0.0003$, 0.0006; $t = -5.802$, −5.302, 7.453, 6.637 respectively). Bottom, one-way ANOVA ($P = 1.75\times10^{-5}$, $F = 24.80$) and post hoc test. (**g–i**) Spontaneous firing in L2/3 neurons in different states. (**g**) Top, records of spontaneous spikes of a L2/3 excitatory cell. Bottom, simultaneously recorded plate rotation speed. Arrow indicates speed at 0. Right inset, superimposed 500 individual spikes. (**h**) Average spontaneous spike rates in the same cell. Bar = s.d. One-way ANOVA ($P = 1.26\times10^{-5}$, $F = 12.88$, $n = 30$ 5-sec segments.) and post hoc test. (**i**) Summary of 17 recorded L2/3 excitatory cells. Spike rate was normalized by the average value in the "Q" state. One-way ANOVA ($P = 2.66\times10^{-7}$, $F = 21.10$) and post hoc test. (**j–l**) Spontaneous spikes recorded in L4 excitatory cells. Data are presented similarly as in (**g–i**). (**k**) One-way ANOVA ($P = 0.9841$, $F = 0.0160$, $n = 28$ segments) and post hoc test. (**l**) One-way ANOVA ($P = 0.1542$, $F = 1.955$, $n = 15$) and post hoc test. (**m**) Peri-stimulus spike time histogram (PSTH, bin size = 1 ms) for the responses of a L2/3 excitatory cell to CF tones (black lines) in different states. Inset, sample record of evoked spikes by the tone. (**n**) Average evoked spike number per stimulus trial plotted for the same cell. Bar = s.d. One-way ANOVA ($P = 1.21\times10^{-5}$, $F = 12.93$, $n = 25$ trials) and post hoc test. (**o**) Summary of average evoked spike numbers for 17 similarly recorded L2/3 excitatory cells. One-way ANOVA ($P = 1.89\times10^{-5}$, $F = 13.76$) and post hoc test. (**p–q**) Evoked spike responses of a L4 excitatory cell. $N = 25$ trials. One-way ANOVA ($P = 0.7415$, $F = 0.3004$) and post hoc test. (**r**) Summary of average evoked spike numbers for 15 recorded L4 cells. One-way ANOVA ($P = 0.1708$, $F = 1.844$) and post hoc test.

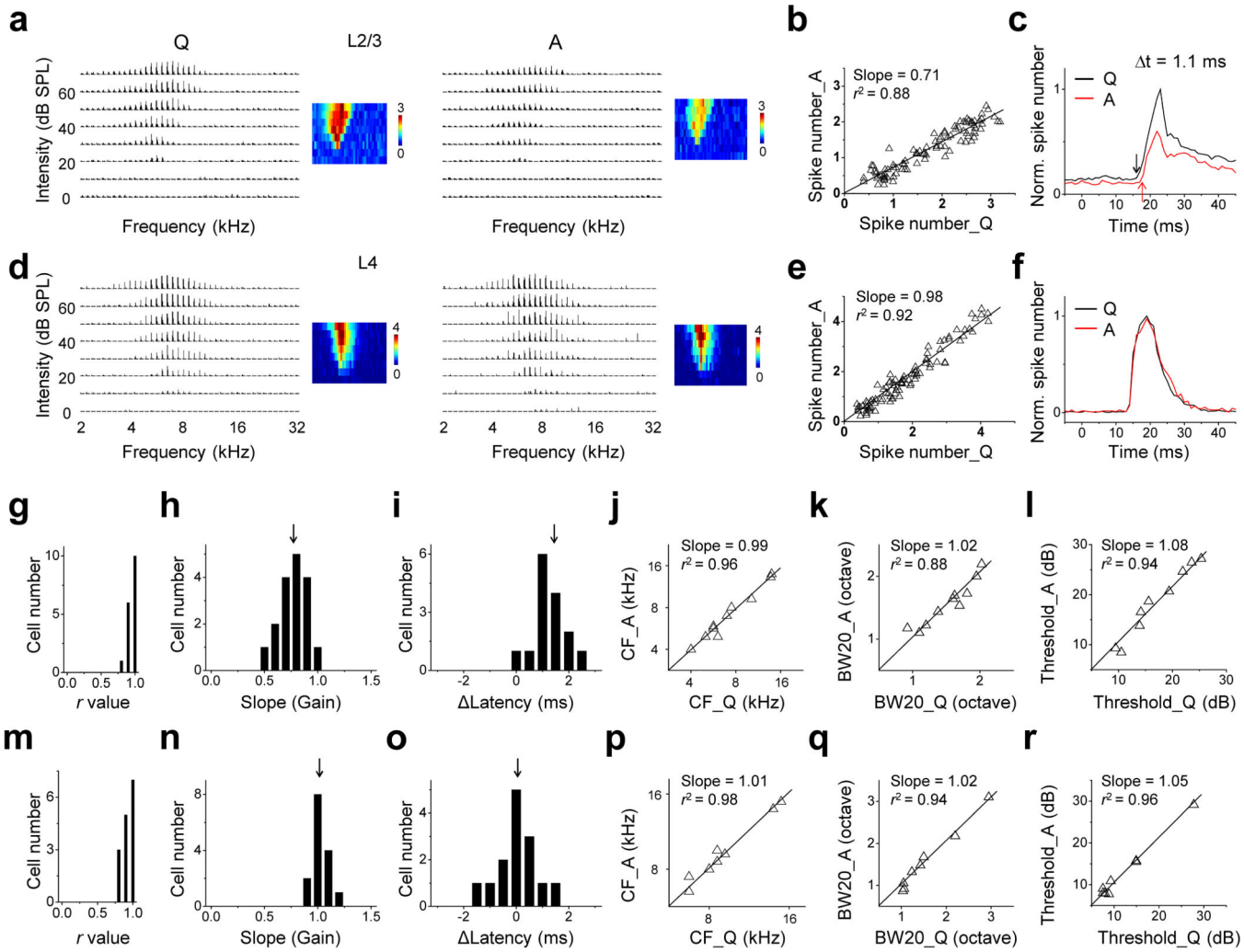

Figure 2.

Gain modulation of auditory responses by behavioral state. (**a**) TRFs of spike responses of a L2/3 cell in quiescence (Q) and active (A) states. Each element in the array represents the PSTH of evoked spikes (60 ms time window, bin size = 2 ms, 10 repeats) to the corresponding tone stimulus. Color map depicts the average spike number evoked by tones. (**b**) Evoked spike number by a tone in active state plotted against that by the same stimulus in quiescence, for the cell shown in (**a**). The best-fit linear regression line is shown. (**c**) Normalized PSTHs for all the tone responses in two states, for the cell shown in (**a**). Arrows indicate response onsets. Δt is the onset difference. (**d–f**) TRFs of a L4 cell. Data are presented in the same way as in (**a–c**). (**g**) Distribution of correlation coefficients (*r*) for all the recorded L2/3 cells. (**h**) Distribution of slopes of the linear regression (i.e. the gain value). Arrow points to the mean value. (**i**) Distribution of differences in onset latency ("A" – "Q") of spike responses. (**j**) Characteristic frequency (CF) of spike TRF in "A" versus "Q" state. The best-fit linear regression line is shown. (**k**) Bandwidth at 20 dB above the intensity threshold (BW20) of spike TRF in "A" versus "Q" state. (**l**) Intensity threshold of spike TRF in "A" versus "Q" state. (**m–r**) Summary for L4 cells. Data are presented in the same way as in (**g–l**).

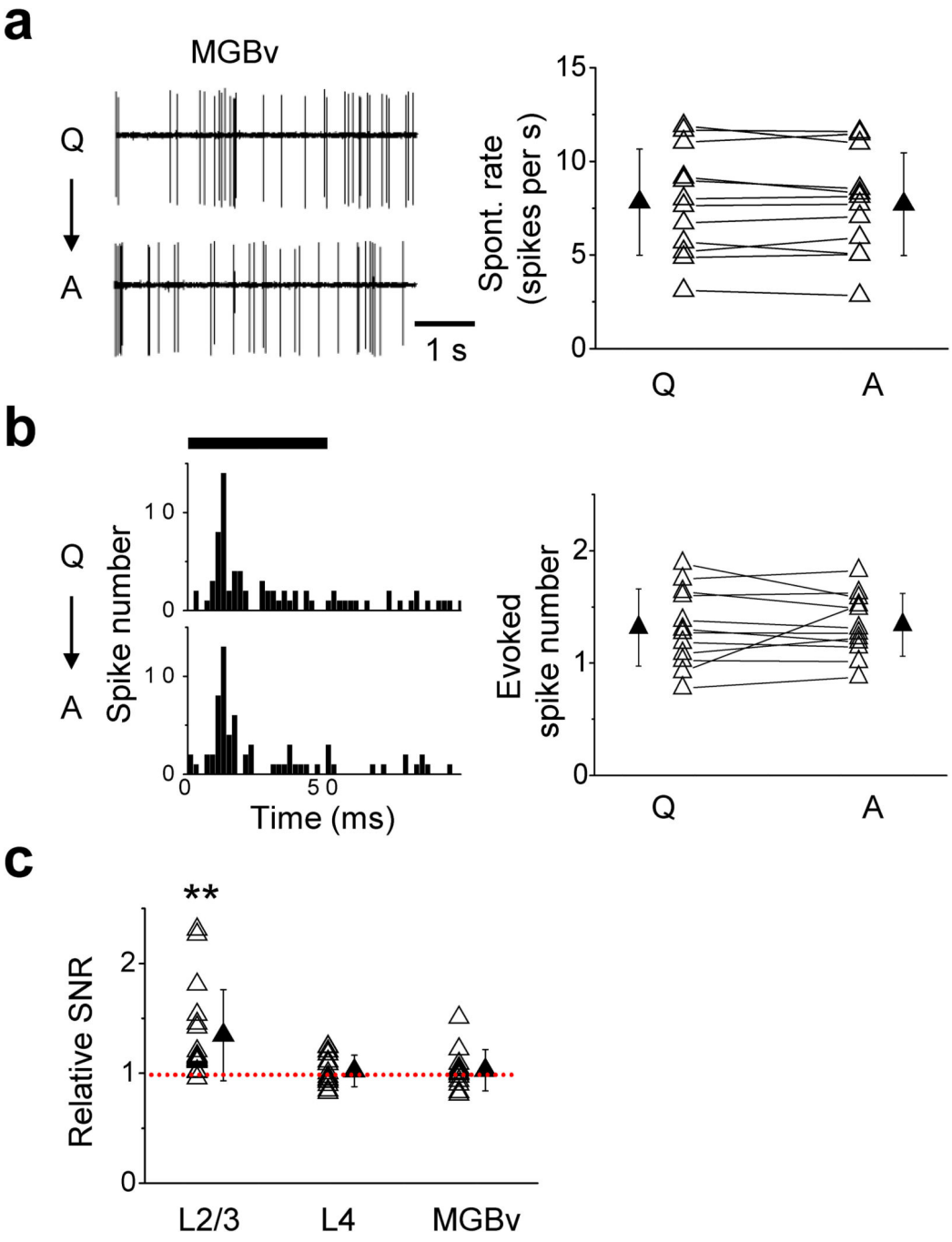

Figure 3.

Activity of thalamic neurons and summary of signal-to-noise ratio (SNR) under different behavioral states. (**a**) Left, sample records of spontaneous spikes in an MGBv neuron in "Q" and "A" states. Right, summary of average spontaneous firing rates (N = 12 cells). Data points from the same cell are connected with a line. Solid symbol represents mean ± s.d. (paired t-test, P = 0.4795, t = 0.7320, n = 12 cells). (**b**) Left, PSTH for CF-tone evoked spikes in different states in the same MGBv neuron as shown in (**a**). Right, summary of average evoked spike numbers by CF tones in different states (paired t-test, P = 0.7640, t =

− 0.3078, n = 12 cells). (**c**) SNR in “A” relative to “Q” state. There is a significant increase in L2/3 cells. From left to right, Wilcoxon signed rank test (**P = 0.0017, Z = 3.435), t-test (P = 0.5834, t = 0.5614), t-test (P = 0.6282, t = 0.4982).

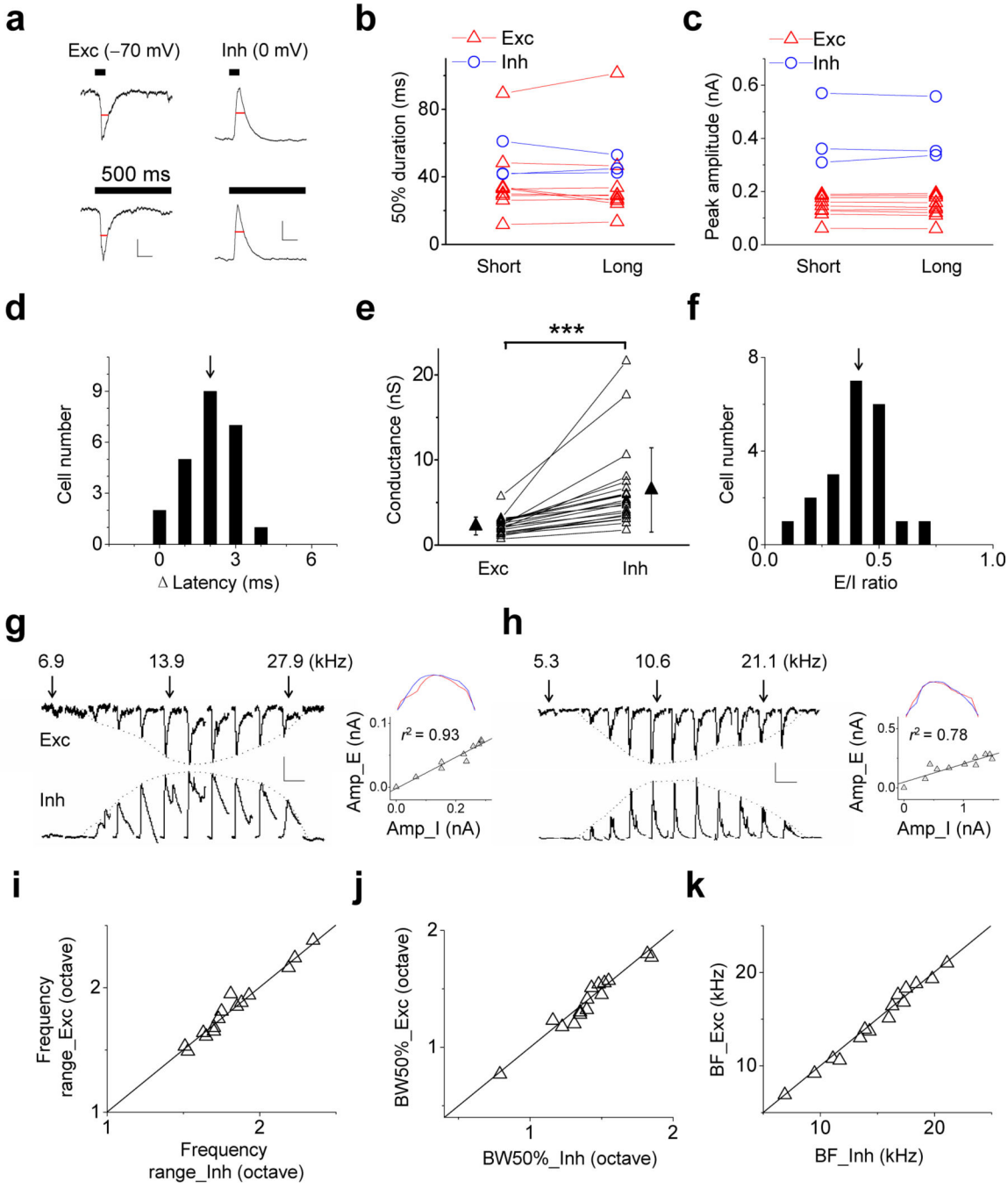

Figure 4.

Properties of synaptic responses in quiescence. (**a**) Average traces of excitatory and inhibitory currents evoked by a best-frequency (BF) tone at 40 dB SPL in an example pyramidal neuron. Black line indicates tone duration. Red line marks 50% duration of the current. Scale: 50 (exc) /100 (inh) pA, 100 ms. (**b**) Durations of BF-tone evoked synaptic currents. Short, 50 ms; long, 200 or 500 ms. Wilcoxon signed-rank test, $P = 0.81, 0.73$; $Z = 0.2439, 0.4024$; $N = 9, 3$ for exc and inh respectively. (**c**) Comparison of peak amplitudes (paired t-test, $P = 0.4, 0.89$; $t = 0.8876, 0.1520$; $N = 9, 3$ for exc and inh respectively). (**d**)

Differences in excitatory and inhibitory onset latency (Inh – Exc). Arrow points to the mean value. (**e**) Comparison of peak amplitudes. Wilcoxon signed-rank test, ***$P = 0.0001$, $Z = -4.464$, $n = 21$. (**f**) Distribution of E/I ratios of peak conductances. (**g**) Frequency tuning of excitation and inhibition in an example cell. Left, average excitatory and inhibitory currents to tones at different frequencies (interval, 0.2 octave). Scale: 30 (exc) / 100 (inh) pA, 200 ms. Right, peak amplitude of excitatory versus inhibitory current evoked by the same stimulus. Top inset, superimposed normalized frequency tuning curves for excitation (red) and inhibition (blue). (**h**) Another example cell plotted similarly as in (**g**). Scale: 100 (exc) / 500 (inh) pA, 200 ms. (**i–k**) Comparison of frequency range (**i**), half-peak bandwidth (**j**), and BF (**k**) between excitation and inhibition in the same cell ($P = 0.52, 0.56, 0.46$, respectively, paired *t*-test, $n = 15$ cells). The unity line is shown.

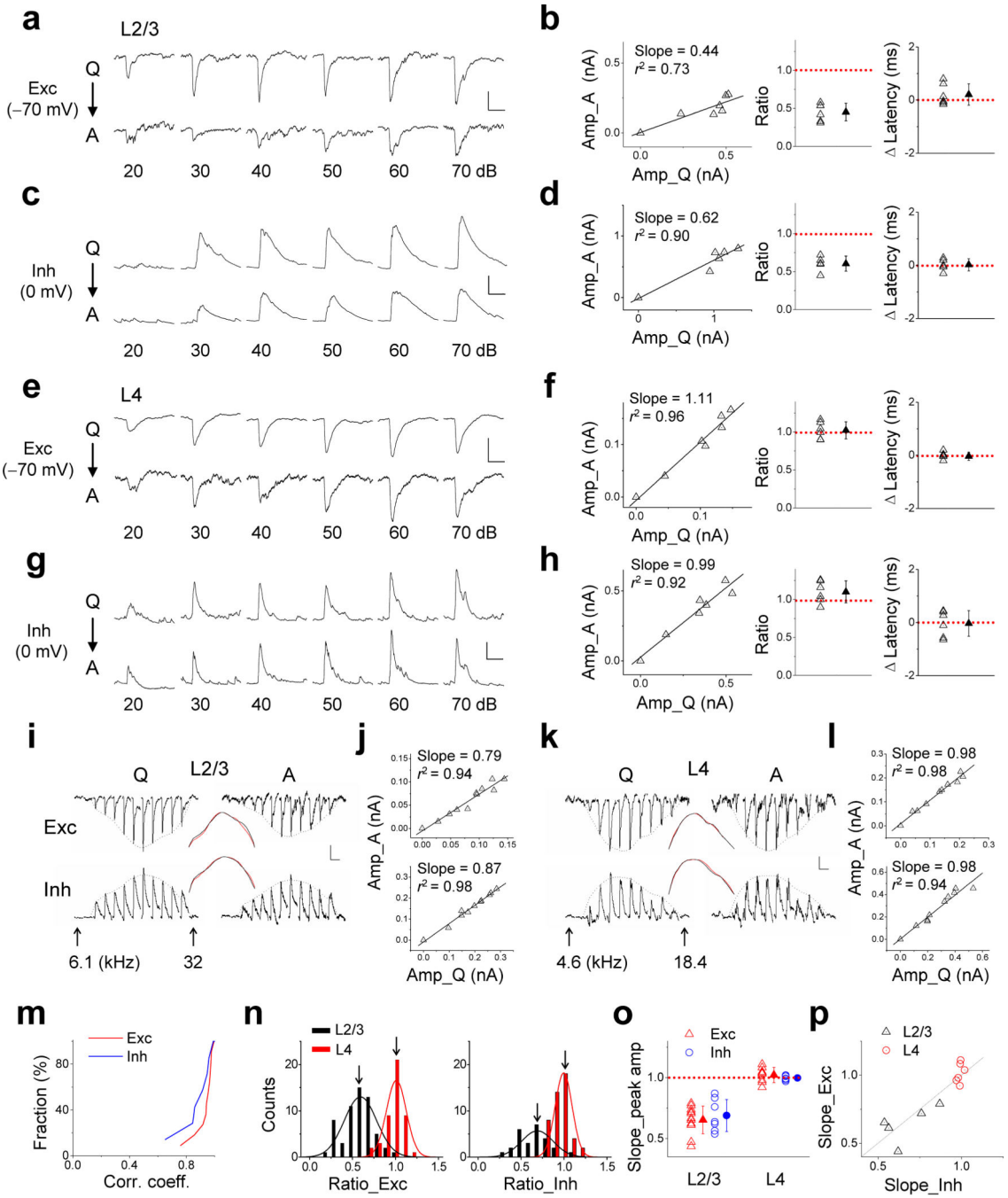

Figure 5.

Modulation of synaptic responses by behavioral state. (**a**) Average evoked excitatory currents to BF tones at different intensities in quiescence and active states in a L2/3 excitatory cell. Scale: 200 pA, 100 ms. (**b**) Left, peak excitatory amplitudes in active versus quiescence state with the best-fit line shown. The near zero point depicts the responses to 10 dB tones not shown in (**a**). Middle, ratio of response amplitudes (Q/A) for all testing intensities (zero responses excluded). Solid symbol represents mean ± s.d. Right, difference in onset latency of evoked synaptic currents (A – Q). (**c–d**) Inhibitory responses in “Q” and

"A" states recorded in the same L2/3 neuron. Scale: 500 pA, 100 ms. (**e–h**) Excitatory and inhibitory responses of a L4 excitatory cell. Scale: 100 pA and 100 ms in (**e**); 200 pA and 100 ms in (**g**). (**i**) Excitatory and inhibitory currents to tones of different frequencies in a L2/3 cell. Scale: 40 (Exc)/ 80 (Inh) pA, 200 ms. Inset, superimposed normalized excitatory (top) and inhibitory (bottom) frequency tuning curves in quiescence (black) and active (red) states. (**j**) Peak response amplitude in active versus quiescence state for the same cell shown in (**i**). Top, excitation; bottom, inhibition. (**k–l**) An example L4 cell plotted in the same manner as in (**i–j**). Scale: 50 (E)/ 150 (I) pA, 200 ms. (**m**) Cumulative distribution of correlation coefficients for synaptic responses in "A" versus "Q" state for L2/3 neurons. (**n**) Distribution of ratios between peak synaptic amplitudes in "A" and "Q" states (A/Q) for all tone stimuli in all recorded cells. Arrows indicate mean values. Left, excitation; right, inhibition. (**o**) Slopes (scaling factors) of the linear regression for "A" versus "Q" peak synaptic responses in all recorded cells. No significant difference between scaling factors of excitation and inhibition in L2/3 cells ($P = 0.5481$, $t = 0.6136$, unpaired t-test, $n = 11, 7$ for excitatory and inhibitory respectively). (**p**) The scaling factors for excitatory responses plotted against that for inhibitory responses in the same cell. For L2/3, $P = 0.6177$, $t = 0.5402$, paired t-test, $n = 5$.

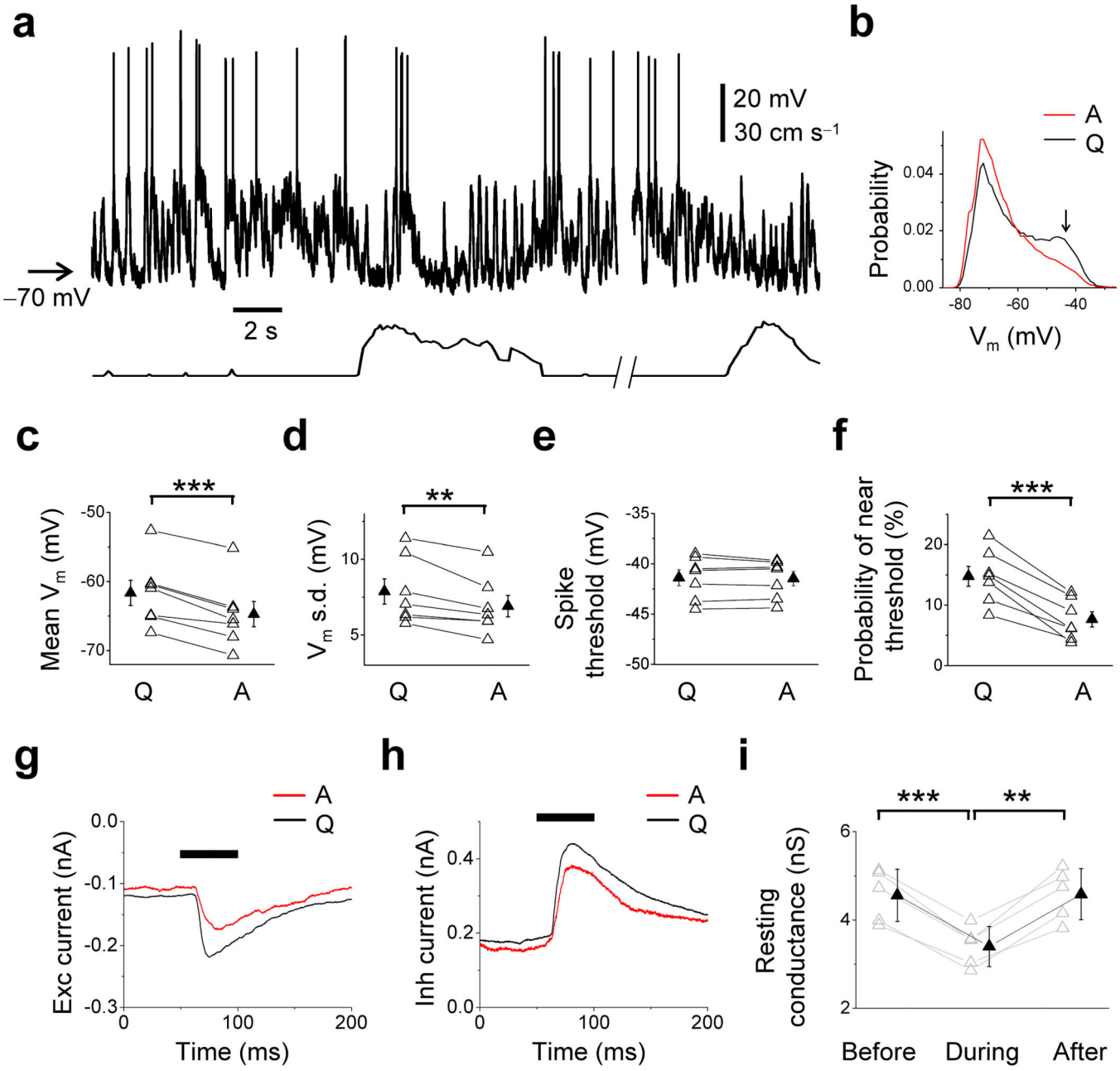

Figure 6.

Modulation of resting membrane potential and resting conductance by behavioral state. (**a**) Sample current-clamp recording records (top) together with the simultaneously recorded speeds (bottom) for an example L2/3 neuron. Arrow labels the level for −70 mV. (**b**) Normalized distribution of membrane voltages during quiescent and active states for the cell shown in (**a**). Arrow points to the average spike threshold of the cell. (**c–f**) Comparison of mean resting membrane potential (**c**), s.d. of resting V_m (**d**), spike threshold (**e**) and percentage of V_m values near spike threshold (not lower than the threshold by more than 10 mV) (**f**) under different behavioral states for 7 recorded L2/3 neurons. Bar = s.e.m., paired *t*-test (***P = 0.0002, **P = 0.0083, P = 0.5496, ***P = 0.0002; t = 8.114, 3.862, 0.6338,

8.139 for (**c–f**) respectively). (**g**) Average excitatory currents of an example cell in response to BF tones (70 dB SPL) in different states. Thick black line marks tone duration. (**h**) Average inhibitory currents of the same cell. (**i**) Resting conductances right before, during and after an epoch of active behaviors for five L2/3 cells. Data points from the same cell are connected by lines. $N = 5$, bar = s.d., paired t-test (***$P = 0.0004$, **$P = 0.0015$; $t = 10.65$, − 7.810)

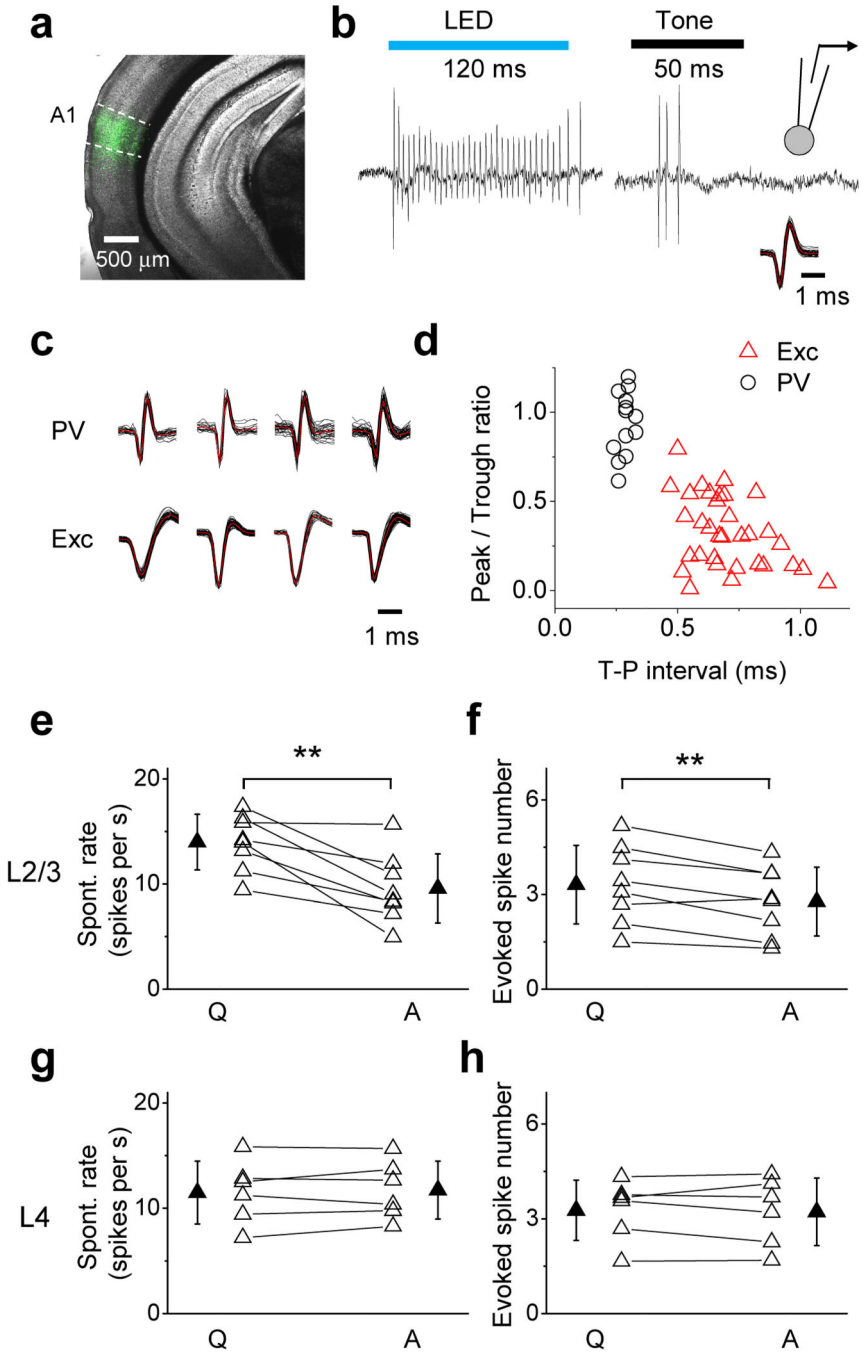

Figure 7.

Changes of activity of PV neurons between different behavioral states. (**a**) Confocal image of a brain section showing ChR2-EYFP expression in the A1 region. (**b**) Left, sample loose-patch recording trace showing a train of evoked spikes of a PV cell to blue LED illumination (marked by the blue bar). Right, sample spike response of the same cell to CF-tone stimulation. Top inset, schematic drawing of loose-patch of a cell. Bottom inset, superimposed 500 individual spikes (black) and the average spike shape (red) of the cell. (**c**) Spike waveforms of four more PV and excitatory cells. (**d**) Plot of peak to trough amplitude

ratio versus trough-to-peak interval for average spike waveforms of PV and excitatory cells recorded with loose-patch methods. Optogenetically identified PV cells were labeled by open circles. (**e**) Summary of spontaneous firing rates of recorded L2/3 PV cells in different states. Bar = s.d.. $N = 8$ cells. $^{**}P = 0.0044$, $t = 4.140$, paired t-test. (**f**) CF-tone evoked spike numbers for the cells in (**e**). $^{**}P = 0.0047$, $t = 4.086$, paired t-test. (**g**) Summary of spontaneous firing rates for PV cells recorded in L4. $P = 0.5013$, $t = -0.7243$, paired t-test, $n = 6$ cells. (**h**) CF-tone evoked spike numbers for the cells in (**g**). $P = 0.7286$, $t = 0.3671$, paired t-test.

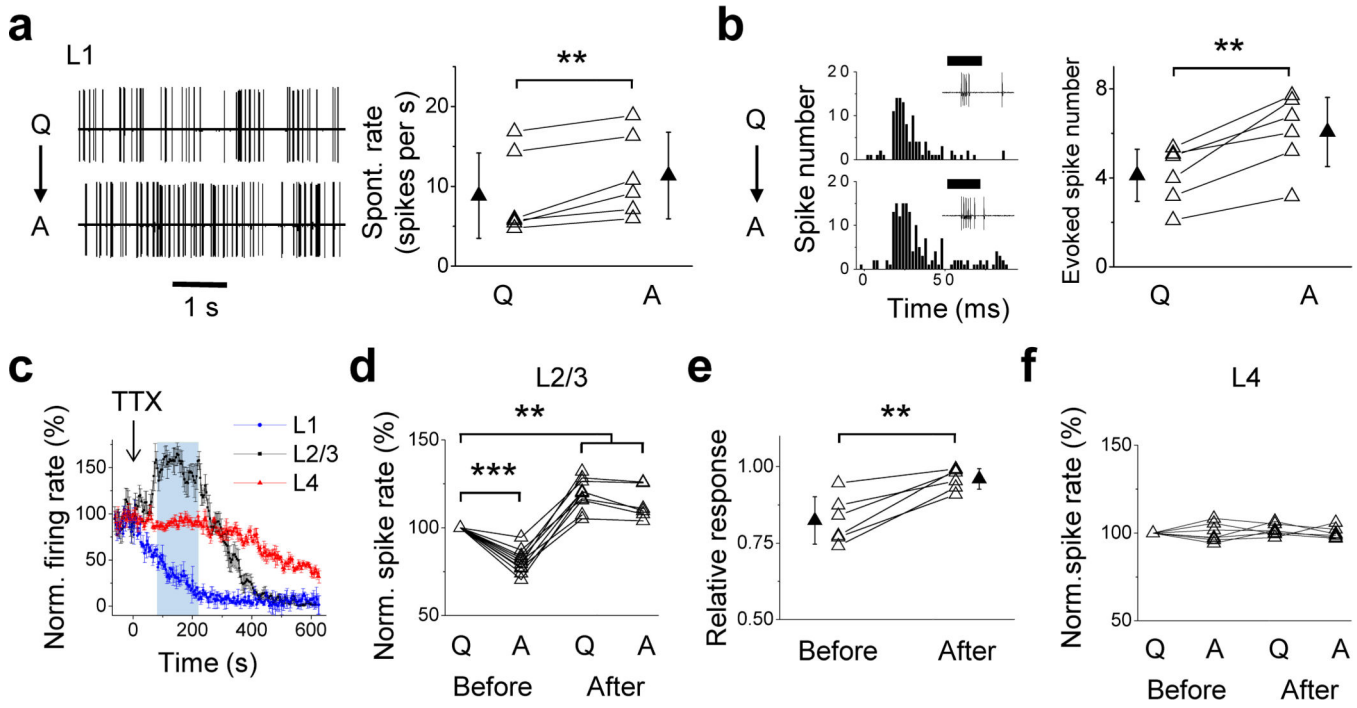

Figure 8.

Role of L1 in the behavioral state-dependent L2/3-specific gain modulation. (**a**) Left, spontaneous spikes of a L1 neuron in different states. Right, summary of average spontaneous firing rates for 6 L1 neurons. Solid symbol represents mean ± s.d. $^{**}P$ = 0.0081, t = −4.252, paired t-test. (**b**) Left, PSTH for CF-tone evoked spikes of the same cell as in (**a**). Right, summary of evoked spike numbers for 6 L1 neurons. $^{**}P$ = 0.0019, t = −5.085, paired t-test. (**c**) Time courses of CF-tone evoked multiunit spike responses in different A1 layers after the topical application of TTX (at time zero). Shaded area denotes the analysis time window during which L2/3 responses were increased to a stable level while L4 responses remained unaffected. N = 4 animals for each layer. Bar = s.d. (**d**) Summary of evoked firing rates of individual L2/3 excitatory cells in different behavioral states before and after TTX application. Spike rates were normalized by “Q” state before TTX application. N = 10 cells. Among these 10 cells, 6 were also recorded in active states after TTX application. $^{**}P < 0.01$, $^{***}P < 0.001$, paired t-test. (**e**) Summary of relative response levels (A/Q) before and after TTX application. $^{**}P$ = 0.0035, t = −5.193, paired t-test, n = 6. (**f**) Summary of normalized evoked spike numbers in different states before and after TTX application for L4 neurons. N = 6 cells.